# Interannual Changes of Stratospheric Water Vapor and Correlations with Tropical Tropopause Temperatures

WILLIAM J. RANDEL AND FEI WU

*National Center for Atmospheric Research, Boulder, Colorado*

SAMUEL J. OLTMANS AND KAREN ROSENLOF

*National Oceanic and Atmospheric Administration, Boulder, Colorado*

GERALD E. NEDOLUHA

*Naval Research Laboratory, Washington, D.C.*

(Manuscript received 21 August 2003, in final form 7 April 2004)

ABSTRACT

Interannual variations of stratospheric water vapor over 1992–2003 are studied using Halogen Occultation Experiment (HALOE) satellite measurements. Interannual anomalies in water vapor with an approximate 2-yr periodicity are evident near the tropical tropopause, and these propagate vertically and latitudinally with the mean stratospheric transport circulation (in a manner analogous to the seasonal ''tape recorder''). Unusually low water vapor anomalies are observed in the lower stratosphere for 2001–03. These interannual anomalies are also observed in Arctic lower-stratospheric water vapor measurements by the Polar Ozone and Aerosol Measurement (POAM) satellite instrument during 1998–2003. Comparisons of the HALOE data with balloon measurements of lower-stratospheric water vapor at Boulder, Colorado (40°N), show partial agreement for seasonal and interannual changes during 1992–2002, but decadal increases observed in the balloon measurements for this period are not observed in HALOE data. Interannual changes in HALOE water vapor are well correlated with anomalies in tropical tropopause temperatures. The approximate 2-yr periodicity is attributable to tropopause temperature changes associated with the quasi-biennial oscillation and El Niño–Southern Oscillation.

## 1. Introduction

Stratospheric water vapor is controlled to a high degree by temperatures near the tropical tropopause. Brewer (1949) suggested that the extreme dryness of the stratosphere is due to a global-scale circulation originating in the Tropics, wherein air entering the stratosphere is freeze dried when crossing the cold tropical tropopause. Striking confirmation of this relationship is provided by the observed annual cycle in stratospheric water vapor coupled to the annual cycle in tropical temperatures (the tropical ''tape recorder''; Mote et al. 1996). While the details of the dehydration process(es) near the tropopause remain a topic of debate (e.g., Dessler 1998; Holton and Gettelman 2001; Sherwood and Dessler 2001), the large coherent annual cycles (~5 K in temperature, and ~1–2 ppmv in water vapor) are strong evidence that stratospheric water vapor responds to temperatures near the tropopause.

Long-term balloon measurements of lower stratospheric water vapor at Boulder, Colorado (40°N), have shown positive trends of ~1% $yr^{-1}$ for the period 1980–2000 (Oltmans et al. 2000), and these positive trends can have significant radiative and chemical effects if representative of the global stratosphere (e.g., Forster and Shine 1999; Dvortsov and Solomon 2001; Shine et al. 2003). Somewhat less than half of this trend can be explained by observed trends in tropospheric methane (oxidized to form water vapor in the stratosphere), but the majority of the observed increase in these data remains unexplained (Kley et al. 2000; Rosenlof 2002). One logical mechanism for the additional increase would be a warming of the tropical tropopause (the cold trap region); a net increase of ~1 K $decade^{-1}$ would be sufficient to explain the observed water vapor trends. However, observations of long-term changes show that the tropical tropopause has *cooled* slightly during the ~1980–2000 time period (Randel et al. 2000; Zhou et al. 2001; Seidel et al. 2001), discounting this as a mechanism for decadal-scale water vapor increases. Thus while stratospheric water and tropopause temperatures are strongly correlated for the (large amplitude) seasonal

*Corresponding author address:* Dr. William J. Randel, NCAR, P.O. Box 3000, Boulder, CO 80307-3000.
E-mail: randel@ucar.edu

cycle, they appear uncorrelated for decadal-scale changes.

The objective of this paper is to use the long record (1991–2003) of near-global satellite observations from the Halogen Occultation Experiment (HALOE) to explore interannual variability of stratospheric water vapor, and furthermore to quantify correlations between the observed water vapor changes and temperatures near the tropical tropopause. We include some comparisons between the HALOE data and Polar Ozone and Aerosol Measurement (POAM) III measurements of water vapor in the Arctic stratosphere during 1998–2003. These two satellite datasets show good agreement for interannual changes during the overlap period, and this supports reliability of the global changes observed by HALOE. We also include comparisons between the HALOE data and updated time series of the Boulder balloon measurements for the region ~16–27 km. In particular we compare interannual variations and long-term changes (trends) for the overlap period 1992–2002.

A main objective here is to quantify the interannual correlations between the HALOE water vapor anomalies and temperatures near the tropical tropopause. We consider temperature records derived from several datasets: meteorological analyses, radiosondes, and satellite measurements. Each of these datasets has strengths and weaknesses in terms of homogeneity and spatial sampling (discussed in detail in section 2), and we find significant differences in derived temperature anomalies, especially at 100 hPa (near the tropical tropopause). Based on the most continuous and homogeneous datasets, we find strong correlations between the water vapor anomalies and tropopause temperatures in the deep Tropics (~10°N–10°S). Origins of the tropopause temperature anomalies can be traced primarily to the stratospheric quasi-biennial oscillation (QBO), along with some influence from the strong-tropospheric El Niño–Southern Oscillation (ENSO) event, which occurred during 1997–98. These coherent variations provide clear evidence for coupling between meteorological climate variability and global stratospheric water vapor.

## 2. Water vapor data

### *a. HALOE water vapor*

The HALOE instrument provides high quality vertical profiles of stratospheric water vapor derived from solar occultation measurements (Russell et al. 1993; Harries et al. 1996). HALOE began operating in October 1991 and continues to the present (early 2004). We use the v19 retrieval product obtained in so-called level-3 format. The HALOE measurements extend from the approximate local tropopause level to above 50 km; the vertical resolution is ~2 km, but the level-3 data are slightly oversampled with a 1.3-km vertical spacing (12 standard levels per decade of pressure, e.g., 100, 82.5, 68.1, . . . hPa). The HALOE occultation sampling makes approximately 15 sunrise and 15 sunset measurements per day, with sunrises and sunsets usually separated in latitude. The latitudinal sampling progresses in time so that it takes approximately 1 month to sample the latitude range ~60°N–60°S (see Russell et al. 1993). We bin the combined sunrise and sunset data into monthly samples for further analyses, and interpolate across missing months in the time series shown here. Extensive intercomparisons with aircraft and balloon measurements in the Stratospheric Processes and Their Role in Climate (SPARC) Water Vapor Assessment (Kley et al. 2000) shows overall high quality for HALOE data, with only a slight dry bias in the lower stratosphere (~5%–20%). We also make use of HALOE methane ($CH_4$) measurements, and their validation is discussed in Park et al. (1996).

Several details of the HALOE water vapor data are relevant, especially for examining long-term changes. The water vapor retrievals are more uncertain in the enhanced stratospheric aerosol environment following the 1991 Mt. Pinatubo volcanic eruption (Hervig et al. 1995). We screen these data by using only profiles where the retrieval uncertainty is less than 10%, and this effectively causes a loss of data in the lowest stratosphere until late 1992. The HALOE retrievals also utilize temperature profiles from National Centers for Environmental Prediction (NCEP) Climate Prediction Centers (CPC) data (see section 3b) below 32 km for pressure registration and other effects, so that erroneous temperature changes could bias retrievals. However, the CPC temperature data do not exhibit unusual changes (as discussed below), so that this is probably not a factor in the HALOE water vapor changes.

### *b. POAM water vapor*

The POAM III instrument (Lucke et al. 1999) is a space-based visible/near-infrared solar occultation photometer on the SPOT satellite. *SPOT-4* was launched in March 1998 and measurements have been available since April 1998. The POAM instrument is on a polar-orbiting satellite (SPOT), and this allows occultation measurements only over high latitudes (~55°–70°N, and ~65°–85°S). Variations in lower stratospheric water vapor over the Arctic are controlled by transport from tropical latitudes (Randel et al. 2001; Nedoluha et al. 2002), whereas in situ dehydration dominates in the Antarctic. Our comparisons here focus on the Arctic POAM measurements. The POAM III water vapor retrievals have an altitude range of ~10–45 km (Lumpe et al. 2002). Validation of these data is discussed in Danilin et al. (2002) and Nedoluha et al. (2002). The primary uncertainty in the POAM III water vapor retrievals in the lower stratosphere is the modeling of aerosol effects; in order to limit errors, we exclude data when the aerosol to water vapor extinction ratio exceeds 15 (Nedoluha et al. 2000).

### c. Boulder balloon water vapor

An ongoing long-term measurement program for stratospheric water vapor has been maintained at Boulder, Colorado (40°N, 105°W), since 1980, using a balloon-borne frost point hygrometer (Oltmans et al. 2000). These balloon measurements are made approximately once per month, and sample altitudes of ~5–25 km with 0.2-km vertical resolution. An individually calibrated instrument is flown for each sounding, together with a radiosonde for temperature and pressure information. The calibration is based on a National Institute of Standards and Technology (NIST) traceable measurement of the frost-point temperature that is converted to mixing ratio (Voemel et al. 1995). In the SPARC Water Vapor Assessment (Kley et al. 2000), good agreement was found with HALOE with a bias of 5% [Climate Monitoring and Diagnostics Laboratory (CMDL) hygrometer lower] in the 10–50-hPa altitude range, but with a somewhat larger difference of 12% with the CMDL hygrometer higher at 60–100 hPa.

## 3. Temperature data

Temperature data analyzed here include meteorological analyses, radiosondes, and satellite datasets, which have varying degrees of spatial coverage, vertical resolution, and time continuity; these are described briefly in turn below. We include these various datasets because they exhibit some substantial differences in derived temperature anomalies near the tropical tropopause, which in turn influence our interpretation of water vapor variability.

### a. Met Office stratospheric analyses

Daily stratospheric analyses have been produced at the Met Office since October 1991 using a stratosphere–troposphere data assimilation system (Swinbank and O'Neill 1994). These data are output on standard pressure levels with six equally spaced levels per decade of pressure, including 100, 68.1, 46.4, . . . hPa. The stratospheric analyses were originally produced as correlative data for the Upper Atmosphere Research Satellite (UARS) project; in October 1995 the separate UARS assimilation system was discontinued, but stratospheric analyses were continued as part of the Met Office operational forecasting suite. Since November 2000 the Met Office stratospheric analyses (METO) have been produced using a 3D variational data assimilation (3DVAR) system (Lorenc et al. 2000), and one important change is that satellite radiance measurements were assimilated directly rather than using retrieved temperature profiles.

A major input to global meteorological analyses [including METO, NCEP, European Centre for Medium-Range Weather Forecasts (ECMWF) 40-yr reanalysis (ERA-40) and CPC data used here] are radiances or temperature profiles from operational satellite measurements. A series of National Oceanic and Atmospheric Administration (NOAA) satellites has been in orbit since 1978, containing a suite of instruments that are collectively called the Television Infrared Observational Satellite (TIROS) Operational Vertical Sounder (TOVS; Smith et al. 1979). An improved set of temperature and humidity sounders called the Advanced TOVS (ATOVS) is now replacing the older TOVS series, beginning with the *NOAA-15* satellite launched in May 1998. Because the TOVS and ATOVS instruments are not identical, there could be discontinuities in analyzed temperature datasets associated with the switch from TOVS to ATOVS measurements. TOVS data were used exclusively in the stratospheric METO analyses prior to the introduction of 3DVAR (November 2000). Both TOVS (*NOAA-14*) and ATOVS (*NOAA-15*) radiances were used after this time until TOVS were replaced by ATOVS (*NOAA-16*) in April 2001.

### b. Climate Prediction Center

Operational daily analyses of stratospheric temperatures have been produced by the Climate Prediction Center of the U.S. National Centers for Environmental Prediction since late 1978 (Gelman et al. 1986). Data for stratospheric pressure levels 70, 50, 30, . . . hPa are based on objective analysis of satellite data (plus radiosondes over Northern Hemisphere midlatitudes). These data are combined with the NCEP operational analyses over 1000–100 hPa, and this latter analysis system evolves over time as improvements are made (e.g., Trenberth and Olsen 1988). The CPC stratospheric analysis system was changed in May 2001, with data up to 10 hPa based on NCEP operational analyses, and satellite data above.

### c. NCEP–NCAR reanalysis

The NCEP–National Center for Atmospheric Research (NCAR) reanalysis project uses a global numerical weather analysis/forecast system to perform data assimilation using historical observations, spanning the time period from 1948 to the present (Kalnay et al. 1996; Kistler et al. 2001). A key feature of the NCEP–NCAR reanalysis is that the analysis system remains constant, although changes in data quality and availability strongly influence the analyses (especially in the lower stratosphere, e.g., Santer et al. 1999). The tropical tropopause region is especially sensitive to the details of data inclusion (W. Ebisuzaki 2003, personal communication). For example, the inclusion of satellite temperature retrievals from TOVS beginning in late 1978 resulted in a jump in analyzed tropical tropopause temperatures by ~2 K (Pawson and Fiorino 1999; Randel et al. 2000). The NCEP–NCAR reanalysis switched from TOVS to ATOVS data in July 2001, and this may have contrib-

uted to the apparent jump in tropical 100-hPa temperatures after 2001 discussed below.

### *d. ERA-40*

The ECMWF has produced a global reanalysis for the period 1957–2002, including the stratosphere up to 1 hPa, based on the use of variational data assimilation techniques. ERA-40 directly assimilates TOVS and ATOVS radiances, as opposed to retrieved temperature profiles. Documentation of the ERA-40 assimilation system and selected data are available on the ECMWF Web site (http://www.ecmwf.int).

### *e. Radiosondes*

Temperature measurements from tropical radiosonde observations are included here, including 23 stations over latitudes ~20°N–20°S with continuous and, we believe, homogeneous records for ~1991–2002. These stations are a subset of those listed in Randel et al. (2000), and the locations are shown later (in Fig. 14). Monthly means have been derived from daily measurements, including data at standard pressure levels 150, 125, 100, 80, 70 hPa, and at the cold point tropopause (temperature minimum). Anomaly time series from each station have been inspected visually and by comparison with microwave sounding unit (MSU) satellite data, and the analyses presented here have omitted stations or pressure levels with obvious discontinuities. One substantial change at United States–controlled stations occurred with a switch in radiosonde instruments in late 1995, which influenced the radiation correction and lower stratospheric daytime temperatures (Seidel et al. 2001; Elliott et al. 2002); these changes were minimized by using only nighttime observations at these stations. The radiosonde data used here agree well with the so-called ''liberal–conservative (LIBCON)'' adjusted radiosonde dataset discussed in Lanzante et al. (2003), which currently only extends to 1997.

### *f. GPS radio occultation*

High quality tropical temperature profiles have been derived from global positioning system (GPS) radio occultation measurements for several time periods. Time series of data covering April 1995 to February 1997 are available from the GPS Meteorology (GPS/MET) satellite (Kursinski et al. 1996; Rocken et al. 1997), and data since June 2001 are available from the [CHAMP; (Challenging Minisatellite Payload) Wickert et al. 2001] and Satélite de Aplicanciones Cientiíficas–C (SAC-C; Hajj et al. 2004) satellites. The GPS radio occultation data are characterized by high vertical resolution, and show excellent agreement with independent measurements over ~10–30 km (Rocken et al. 1997; Hajj et al. 2004; Randel et al. 2003). A particular strength of the GPS occultation technique is that there are no intersatellite calibration effects on derived temperatures. Although the temporal records are short at present (GPS/MET for 1995–97, and CHAMP and SAC-C for 2001–03), these data allow independent measures of variability for these periods, and are the start of what may well become a key climate monitoring data product for the future.

### *g. MSU-4*

Global satellite measurements from the microwave sounding unit channel 4 (MSU-4) provide a weighted layer mean temperature of the lower stratosphere over approximately 13–22 km (Spencer and Christy 1993). The MSU-4 time series extends from late 1978 to 2002, based on combining results from many operational datasets (e.g., Christy et al. 2000). The MSU-4 measurements used here are from a newly developed dataset from Remote Sensing Systems, Inc. (RSS), as described in Mears et al. (2003).

## 4. Water vapor observations

### *a. Updated HALOE record*

Time variations in near-global average (60°N–60°S) HALOE $H_2O$ at 82 hPa (~17.5 km) are shown in Fig. 1a, covering the period January 1992–August 2003. The 82-hPa level is just above the tropopause in the Tropics, and $H_2O$ exhibits a strong seasonal cycle tied to temperatures near the tropical tropopause (Mote et al. 1996). Interannual variations are also evident in Fig. 1a, and these are highlighted in Fig. 1b by simply deseasonalizing the data (using a harmonic seasonal cycle fit of monthly data at each latitude and height, as in Randel et al. 1998). Two interesting features are evident in the deseasonalized time series (Fig. 1b): 1) there is an approximate 2-yr periodicity in the anomalies, and 2) there are persistent low values observed for the last 3 yr (2001–03). Note these low values are observed during both NH summer and winter in the full data (Fig. 1a).

A height–time section of deseasonalized $H_2O$ anomalies over 20°N–20°S is shown in Fig. 2. Anomalies with an approximate 2-yr periodicity originate at levels near 100 hPa and propagate vertically into the middle stratosphere; note also the vertical propagation of the low anomalies at the end of the record. These patterns are effectively the interannual signal analog of the seasonal tape recorder described by Mote et al. (1996). The $H_2O$ anomalies increase in amplitude above 10 hPa in Fig. 2, with a maximum near 40 km; these upper-stratospheric maxima are primarily related to $CH_4$ oxidation (as shown below), whereas the anomalies below 10 hPa originate near the tropopause. The anomalies in Fig. 2 propagate vertically between 100–10 hPa with a mean speed of ~8 km $yr^{-1}$ (~0.25 mm $s^{-1}$). This value is very similar to the propagation speed of the annual cycle in water vapor (Mote et al. 1998; Niwano et al. 2003),

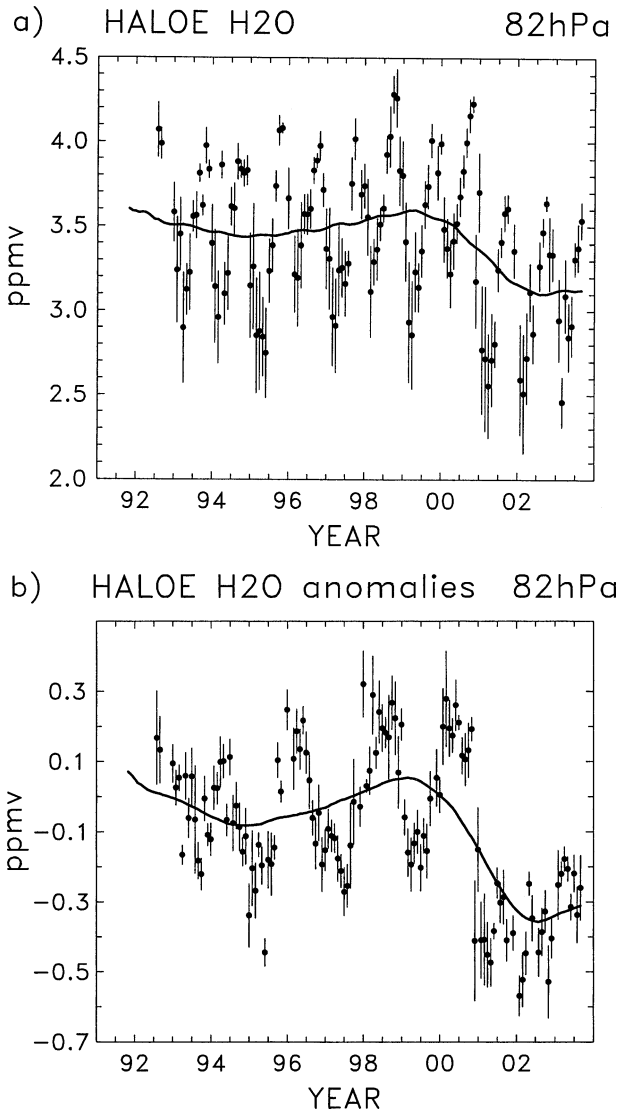


FIG. 1. (a) Time series of near-global mean (~60°N–60°S) water vapor at 82 hPa derived from HALOE data. The circles show monthly mean values, and error bars denote the monthly standard deviation. (b) Deseasonalized near-global mean $H_2O$ anomalies at 82 hPa. The solid lines are running Gaussian-weighted means of the individual points (using a Gaussian half-width of 12 months).

and also close to the calculated mean upwelling rate in the tropical lower stratosphere (Rosenlof 1995). However, as discussed in detail by Waugh and Hall (2002), in general the propagation time (or phase lag) of periodically varying tracers in the tropical stratosphere varies with the period of the cycle, with slower propagation for longer periods. The fact that similar propagation speeds are observed in water vapor for annual and approximately 2-yr variations (Fig. 2) suggests quantitative information on transport that will be explored in future work.

The structure and variability of $H_2O$ and $CH_4$ are tightly coupled in the stratosphere, because $CH_4$ oxidation is a principal source of stratospheric $H_2O$ (e.g., Remsberg et al. 1984). Oxidation reactions in the middle and upper stratosphere produce approximately two molecules of $H_2O$ for every one of $CH_4$, and empirical studies show that the quantity $H_2O + 2 \times CH_4$ is an approximately conserved parameter (away from source–sink regions for $H_2O$; e.g., Dessler et al. 1994). Figure 3 shows a height–time section of $H_2O + 2 \times CH_4$ anomalies over 20°N–20°S derived from HALOE data. This shows nearly identical variability as the $H_2O$ anomalies alone (Fig. 2) below 10 hPa, but substantial dif-

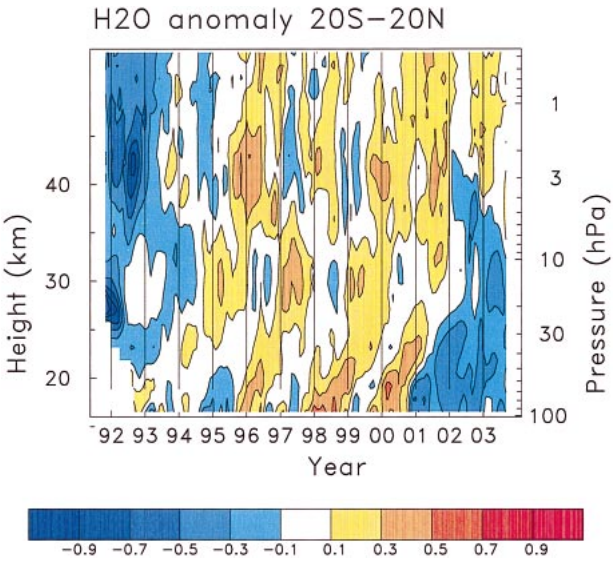


FIG. 2. Height–time cross section of deseasonalized HALOE $H_2O$ anomalies averaged over 20°N–20°S. Contours are ±0.1, 0.3, . . . ppmv (zero contours omitted).

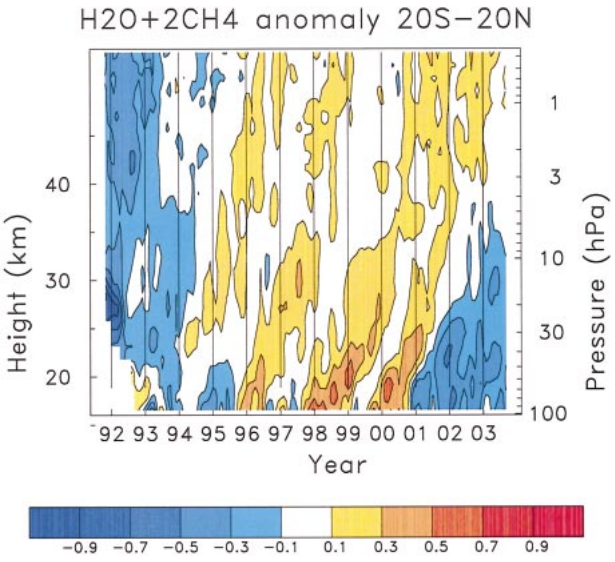


FIG. 3. Height–time cross section of deseasonalized anomalies in $H_2O + 2 \times CH_4$ from HALOE measurements averaged over 20°N–20°S. Contours are ±0.1, 0.3, . . . ppmv.

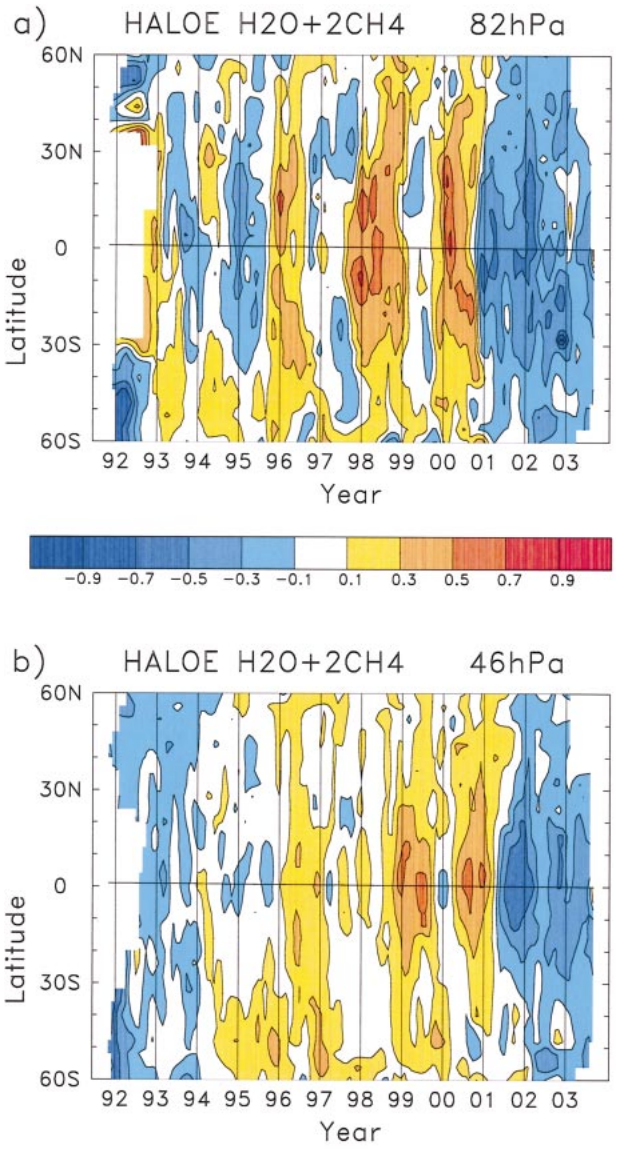


FIG. 4. Latitude–time cross sections of deseasonalized anomalies in $H_2O + 2 \times CH_4$ at (a) 82 hPa and (b) 46 hPa. Contours are $\pm 0.1$, 0.3, . . . ppmv.

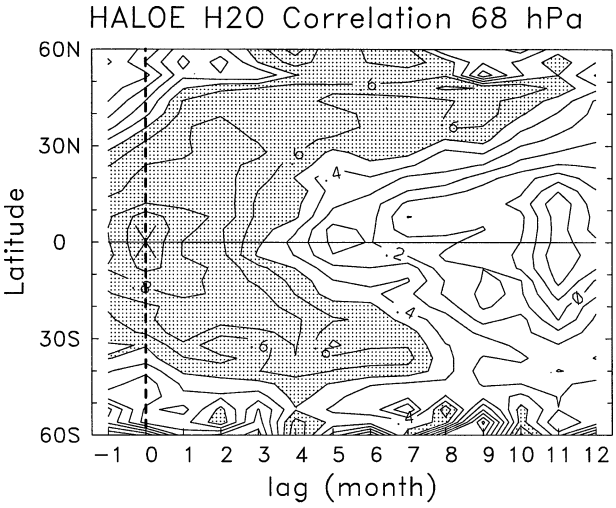


FIG. 5. Latitude–time lag correlation map of deseasonalized $H_2O$ anomalies at 68 hPa, with respect to a reference time series at the equator. Values above 0.5 are shaded. Note the highest correlations spread to midlatitudes of both hemispheres with time lag ~3–6 months.

ferences above; in this case the anomalies decrease monotonically in amplitude away from 100 hPa. A large fraction of the $H_2O$ anomalies above 10 hPa in Fig. 2 originate from $CH_4$ oxidation, and are mirrored in oppositely signed $CH_4$ anomalies (not shown here, but see Figs. 19–21 of Randel et al. 1998). The residual $H_2O + 2 \times CH_4$ anomaly patterns in Fig. 3 show continuous propagation of anomalies from the tropopause up to the stratopause (~50 km), and these continue into the middle mesosphere (not shown here). The magnitude of the anomalies decreases between the tropopause and ~30 hPa (~25 km), and is approximately constant above.

The latitudinal distribution of $H_2O + 2 \times CH_4$ anomalies at 82 hPa is shown in Fig. 4a, and virtually identical patterns are derived for $H_2O$ alone. This shows that the large amplitude anomalies are centered in the Tropics, and have a broad latitudinal structure covering at least ~40°N–40°S. The low 2001–03 anomalies cover nearly the entire globe (60°N–60°S). Figure 4b shows a similar diagram of the $H_2O + 2CH_4$ anomalies at 46 hPa (~22 km), showing patterns delayed by approximately 6 months compared to 82 hPa, and maxima somewhat more confined to the Tropics.

There is some suggestion in Fig. 4 that extratropical anomalies follow those in the Tropics by several months. This is quantified in Fig. 5, which shows a latitude–time lag correlation diagram of $H_2O$ anomalies at 68 hPa with respect to variations at the equator. The correlations show clear propagation of tropical anomalies into midlatitudes of both hemispheres with a time lag of ~3–6 months. This is consistent with the meridional propagation observed of the $H_2O$ seasonal cycle in the lowermost stratosphere (e.g., Randel et al. 2001).

### *b. Comparison with POAM data*

The POAM III instrument has been making measurements of polar stratospheric water vapor since April 1998, and Fig. 6 shows an altitude–time series of the Arctic POAM observations over 10–25 km for 1998–2003. These data span the latitude range of ~55°–70°N. The time series show a strong seasonal minimum (during March–July) over ~14–18 km each year; this relatively dry air originates near the tropical tropopause, and is transported meridionally in the lower stratosphere (approximately following the 380–400-K isentropes) all the way to the polar cap (Randel et al. 2001; Nedoluha et al. 2002). Of more interest here are the interannual variations in water vapor evident in the seasonal minima

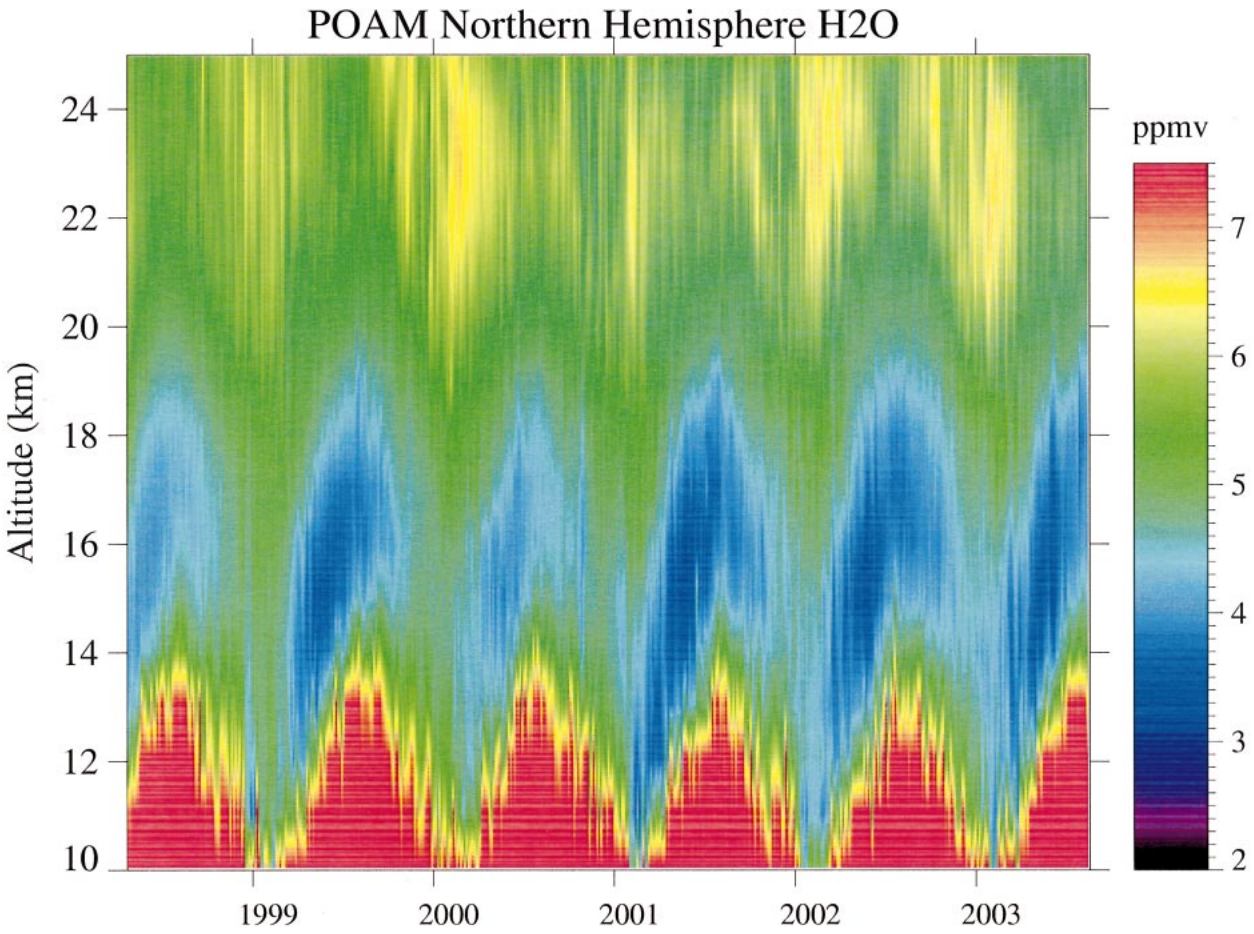


FIG. 6. Height–time section of POAM stratospheric water vapor measurements over the Arctic (latitudes ~55°–70°N) during 1998–2003.

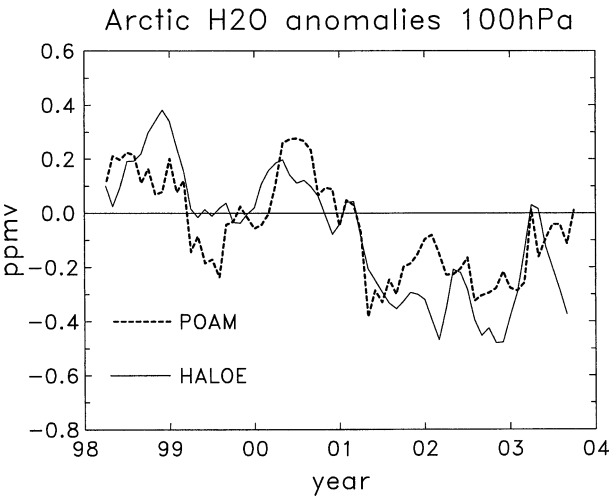


FIG. 7. Time series of deseasonalized anomalies in Arctic water vapor at 100 hPa, derived from POAM and HALOE measurements. POAM data span the latitude range ~55°–70°N, and HALOE data are averaged over 55°–60°N. Both datasets are deseasonalized with respect to the period 1998–2001.

in Fig. 6, namely, relatively shallow minima in 1998 and 2000, and deep minima in 1999 and for the 3 yr 2001–03. Figure 7 shows a comparison of the deseasonalized anomalies in POAM Arctic data at 16 km with HALOE 100 hPa anomalies over 55°–60°N (near the northernmost latitude of regular HALOE measurements, e.g., see Fig. 4). The interannual anomalies in Fig. 7 show overall good agreement between the POAM and HALOE measurements, and in particular both datasets show relatively low water vapor anomalies for the most recent period 2001–03. This agreement is more remarkable when noting the magnitude of the anomalies is ~0.2 ppmv, which is ~5% of background values. This agreement reinforces confidence in the global water vapor anomaly patterns derived from HALOE data alone.

### *c. Comparison with Boulder balloon data*

An updated time series of the Boulder frost-point hygrometer measurements averaged over 17–22 km is shown in Fig. 8. These frost-point data were obtained from an updated and revised dataset provided courtesy

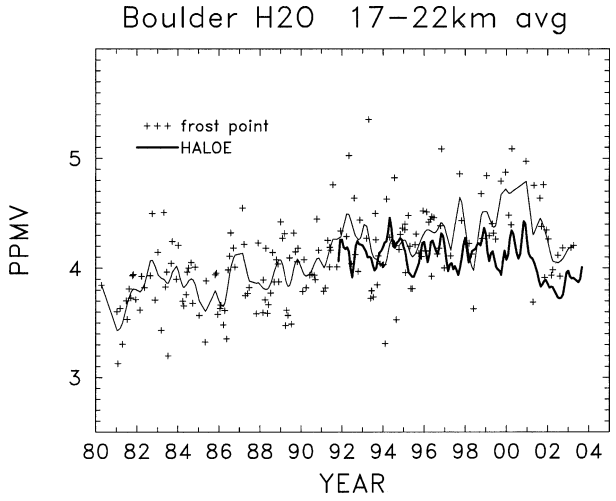


FIG. 8. Data points show time series of water vapor averaged over 17–22 km at Boulder, CO, from frost-point hygrometer measurements covering 1980–2002. The thin line shows a smooth fit through the data points using a running Gaussian window with a half-width of three months. The heavy line shows HALOE satellite water vapor data during 1992–2002 for the same altitude region, using measurements near Boulder (over latitudes 35°–45°N and longitudes 80°–130°W).

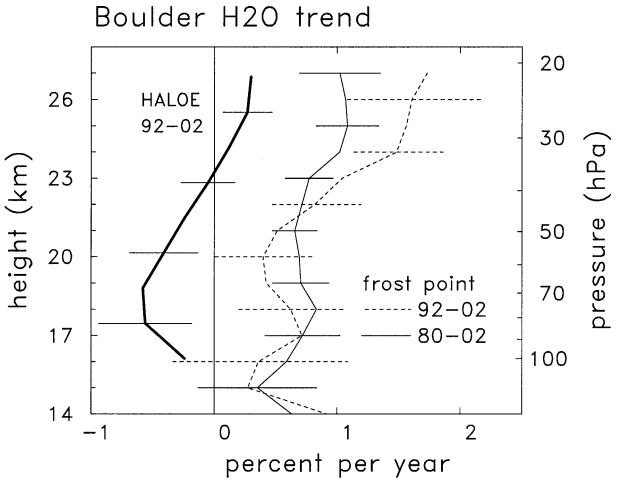


FIG. 9. Vertical profile of linear trends in water vapor derived from the Boulder frost-point hygrometer data (light lines, shown for two time periods 1980–2002 and 1992–2002), and HALOE data for 1992–2002 (dark line). The HALOE trends are based on measurements near Boulder (35°–45°N and 80°–130°W); very similar results are found for zonal means over 35°–45°N. Error bars show the statistical uncertainties of the linear trend fits.

of Holger Voemel (available at http://cires.colorado.edu/~voemel/data/data.html). Figure 8 includes a smooth curve fit through the data to highlight the low-frequency variations (derived using a moving Gaussian window with half-width of 3 months). The long-term increase in water vapor at Boulder is clearly evident, along with a considerable amount of interannual variability [although the latter could be significantly influenced by the infrequent (~ once monthly) sampling]. Figure 8 also shows HALOE water vapor data during 1992–2002, using data averaged over pressure levels 82–46 hPa (~17–22 km), and including measurements near Boulder (over latitudes 35°–45°N and longitudes 80°–130°W; very similar results are found using zonal means over 35°–45°N). There is reasonable agreement between the Boulder and HALOE datasets in Fig. 8 for the early part of the overlap record (1992–96). However, the time series diverge after 1997, with the balloon measurements showing overall higher values than HALOE; note that both datasets show a relative decrease after 2001. Because of the higher values after 1997, the Boulder measurements show an overall $H_2O$ increase for 1992–2002, whereas the HALOE data do not. The difference in long-term changes is quantified in Fig. 9, comparing vertical profiles of the linear trends in Boulder data (for 1980–2002 and 1992–2002) with trends derived from HALOE measurements for 1992–2002. The trend regression calculations include a term to model QBO variability, and statistical uncertainties are estimated using resampling techniques (as in Randel et al. 1999). The balloon data show a statistically significant increase of ~0.5%–1% $yr^{-1}$ over ~15–25 km for both time periods, whereas the HALOE data for 1992–2002 show negative or near-zero trends. The negative ''trends'' for the lowest levels of HALOE data primarily arise from the very low, persistent values occurring at the recent end of the time series (e.g., Figs. 1–4), and a linear trend is not an appropriate statistical model of this short record. Nonetheless, Fig. 9 serves to quantify the significant differences in decadal-scale changes inferred from the Boulder balloon data (increases of ~1% $yr^{-1}$) and HALOE record (near zero or negative trends) for the identical time period 1992–2002.

For reference, Fig. 10 shows a meridional cross section of the global $H_2O$ trends derived from HALOE data for 1992–2002, together with time series of deseasonalized anomalies at 82, 10, and 2 hPa illustrating the actual variability. Figure 10 shows that negative trends cover the global lower stratosphere, but these are simply due to the anomalously low values at the end of the short time series. Conversely, the upper stratosphere shows positive trends, but these are primarily due to anomalously low values at the beginning of the short record (1992–93; see also Fig. 2). The existence of relatively abrupt changes in stratospheric water vapor in the HALOE record cautions against overinterpretation of linear trends calculated from a short record with arbitrary end points. This is reinforced by the changing character of HALOE $H_2O$ trends as the record length increases (e.g., the different results of Nedoluha et al. 1998; Randel et al. 1999; Rosenlof 2002; Nedoluha et al. 2003; and Fig. 10 here). Nonetheless, the large differences between the Boulder and HALOE trends for the same 1992–2002 time period is disconcerting, because these are the two best long-term records of stratospheric water vapor available at present.

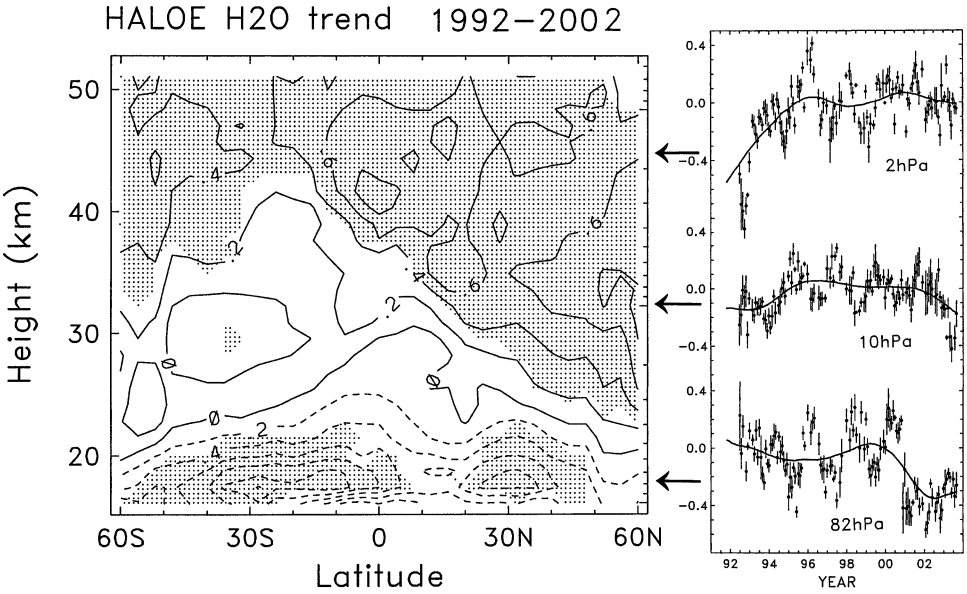


FIG. 10. (left) A meridional cross section of linear trends in HALOE $H_2O$ data for 1992–2002. Contour interval is 0.2% $yr^{-1}$ and shaded regions indicate statistically significant trends. (right) Time series of deseasonalized $H_2O$ anomalies at 2, 10, and 82 hPa, from top to bottom; details of these time series are the same as in Fig. 1b. Note that the derived trends in this short time sample are highly influenced by low-frequency variations at either end of the time series.

## 5. Correlations with tropical tropopause temperatures

Here we consider correlations between the observed HALOE $H_2O$ anomalies over 1992–2002 and temperatures near the tropical tropopause, with the anticipation of finding temperature anomalies as a precursor to the $H_2O$ variability. We use the deseasonalized HALOE $H_2O$ anomalies at 82 hPa over 20°N–20°S (i.e., just above the tropical tropopause) as a reference time series, and explore time series and cross correlations with the several temperature datasets discussed in section 2. We note that nearly identical results are found using $H_2O$ anomalies at 100 hPa; the choice of 82 hPa is based on the fact that the cold point tropopause typically lies between 100 and 82 hPa. Furthermore, this is consistent with the fact that the seasonal cycle in HALOE water vapor shows a minimum at 82 hPa.

Temperature data from meteorological analyses are available on standard pressure levels 150, 100, and 70 hPa; standard radiosonde archives have somewhat higher vertical resolution, adding 125 and 80 hPa, and also include the cold point (seasonally varying between ~90–105 hPa). While the 100-hPa level is in general a poor surrogate for the tropical tropopause (Seidel et al. 2001), it is the closest standard analysis level available from global analyses. Additionally, interannual temperature variations are nearly identical between the cold point tropopause and 100 hPa (Seidel et al. 2001; see also Fig. 13 below).

Significance for the $H_2O$–temperature correlations are estimated as follows. After omitting the first 6 months of 1992 (due to questions of HALOE data quality), the time series covers July 1992–December 2002 ($N = 126$ months). However, both the $H_2O$ and temperature anomaly time series are dominated by low-frequency variability, which significantly reduces the effective number of degrees of freedom. One-month lag autocorrelations for these datasets are typically $r_1 \sim 0.8$, and a simple estimate of the number of independent data points is given by $N(1 - r_1)/(1 + r_1) \sim 14$ (Trenberth 1984). Cross-correlation values of 0.45 and 0.52 are then significant at the 10% and 5% levels, respectively.

Figure 11 shows time series of the deseasonalized temperature anomalies in the deep Tropics (10°N–10°S) at 100 hPa (the standard pressure level closest to the tropopause), including all six temperature datasets discussed in section 2b. Here, the temperatures in each dataset have been deseasonalized using the entire record, and anomalies have been normalized with respect to the time period April 1995–February 1997, in order to directly include the GPS measurements. Figure 11 shows substantial differences in the anomalies at 100 hPa, most notably for the time period 2001–02. During these years the NCEP and METO datasets show large and persistent cold anomalies (of order 2–3 K), whereas the ERA-40, CPC, radiosonde, and GPS datasets do not. These substantial differences in the tropical climate record at 100 hPa (near the tropopause) are especially confusing for interpretation of the water vapor variability; note the period of large 100-hPa differences in Fig. 11 (~2001–02) is precisely the period of the persistent dry anomalies observed in the HALOE $H_2O$ data (e.g., Fig. 1b).

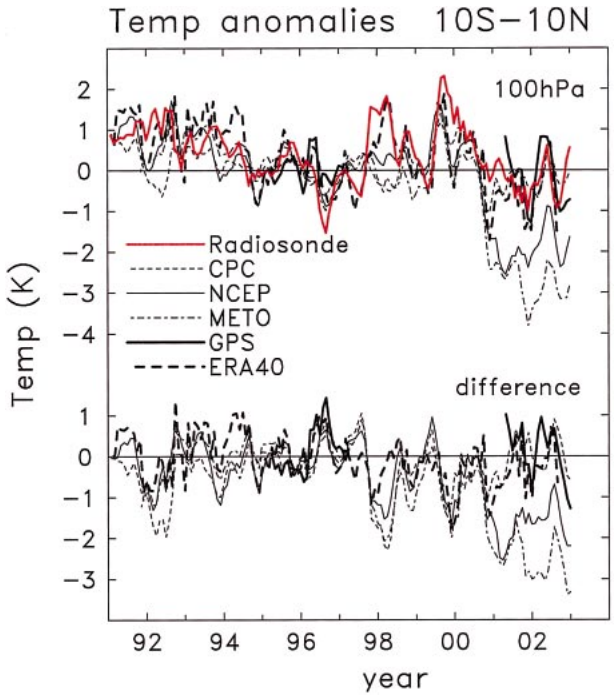


FIG. 11. (top) Time series of deseasonalized 100-hPa temperature anomalies over 10°N–10°S, showing results from six different datasets. Each time series is normalized to be zero for Apr 1995–1997. (bottom) Difference of the respective time series with averaged radiosonde data.

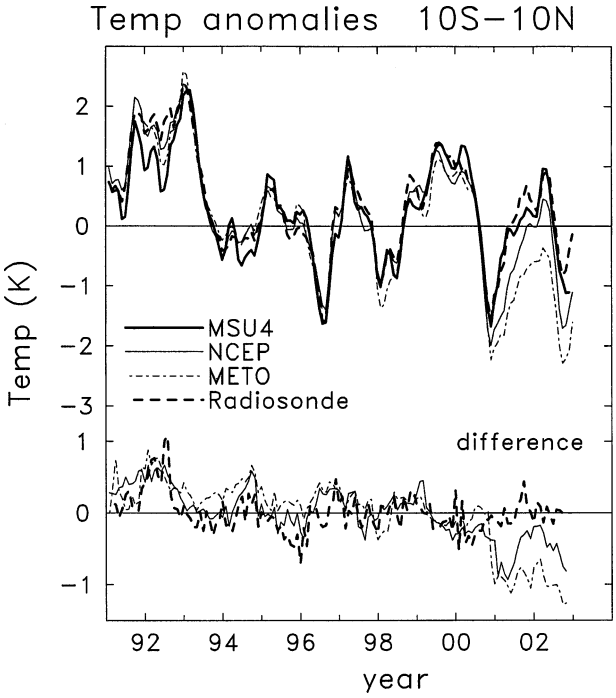


FIG. 12. (top) Time series of deseasonalized temperature anomalies from MSU-4 satellite data, together with corresponding time series derived from NCEP, METO, and radiosonde datasets (vertically integrated using the MSU-4 weighting function); these time series are smoothed with a 1–2–1 running filter. (bottom) The respective differences with respect to MSU-4, with no time smoothing applied.

A complementary dataset for comparison of tropical temperature variability is provided by satellite measurements from MSU-4, which represents a weighted mean layer temperature over ~13–22 km. Figure 12 compares the deseasonalized anomalies in MSU-4 data over 10°N–10°S with vertically integrated profile anomalies from NCEP, METO, and radiosonde data, using the MSU-4 weighting function (i.e., weighted pressure level data, as in Spencer and Christy 1993). Overall the integrated profile data agree reasonably well (to within ~0.5 K) and track all of the variability of the observed MSU-4 anomalies for the time period prior to 2000, whereas both the integrated NCEP and METO data exhibit cold biases during 2001–02 (Calculations for the ERA-40 and GPS data are similar to the radiosonde results, and for clarity, are not included in Fig. 12). Comparisons of the vertical profiles of temperature anomalies during this 2001–02 period (not shown here) furthermore suggest problems in the NCEP and METO data, especially at the 100-hPa level.

The overall comparisons suggest that the cold 100-hPa anomalies seen for 2001–02 in NCEP and METO data (Fig. 11) are erroneous, and probably related to changes in analysis system or input data. The METO stratospheric analysis changed to a 3DVAR system in November 2000, and also began to assimilate radiances rather than retrieved temperature profiles, and this is very close to the time when anomalies appear at 100 hPa and differences with MSU-4 begin (Figs. 11–12). The NCEP–NCAR, reanalysis system has remained constant in time, but there are continually evolving changes in available input data. A potentially important change occurred with the introduction of temperature retrievals from ATOVS satellite measurements in July 2001, although the NCEP–NCAR temperature changes in Figs. 11–12 appear to occur closer to the beginning of 2001 (very similar to METO). Thus, while we are suspicious of the discontinuous behavior in NCEP–NCAR 100-hPa data (and their disagreements with radiosondes, GPS, and MSU temperatures), a clear cause has not been identified.

Correlations between the HALOE lower stratosphere $H_2O$ anomalies over 20°N–20°S and near-tropopause temperature anomalies from the various datasets are listed in Table 1. These include both contemporaneous correlations, and correlations for the water vapor time series lagged by 2 months (this increases the correlation values, consistent with the $H_2O$ anomalies being an integrated response to temperature variations). In the following discussions we refer to these lagged correlation values. The strongest correlation (0.73) is found with the NCEP–NCAR 100-hPa temperatures, but at least part of this arises from the cold anomalies for 2001–02, which is a questionable detail. The radiosonde data show relatively high correlations for pressure levels 100

TABLE 1. Correlations between HALOE 82-hPa $H_2O$ anomalies and 10°N–10°S temperature anomalies at different levels; X's are shown if data are unavailable at that level. The left number in each column refers to the correlation with water vapor lagged by 2 months, while the right (bracketed) value refers to contemporaneous (lag 0) correlations.

| Source | 125 hPa | 100 hPa | Cold point | 80 hPa | 70 hPa |
|---|---|---|---|---|---|
| CPC | X | 0.48 [0.36] | X | X | 0.40 [0.32] |
| METO | X | 0.25 [0.28] | X | X | 0.46 [0.43] |
| NCEP | X | 0.73 [0.68] | X | X | 0.52 [0.44] |
| ERA-40 | X | 0.67 [0.57] | X | X | 0.44 [0.30] |
| Radiosondes (all 10°N–10°S) | 0.06 [−0.07] | 0.61 [0.49] | 0.72 [0.56] | 0.64 [0.49] | 0.48 [0.35] |

and 80 hPa, and an even higher value using the cold point (0.72). Figure 13 shows time series of the 82-hPa water vapor anomalies, together with radiosonde cold point temperatures (averaged for all stations over 10°N–10°S), plus 100-hPa zonal mean temperature anomalies from ERA-40 data (which are virtually identical to the radiosonde cold point anomalies). Beyond the significant numerical correlations, the respective time series show agreement in the timing of large anomalies, for example, warm temperatures and high water vapor for 1997–98 and 1999–2000. The tropical mean temperatures are relatively cold for 2001–02, but the anomalies have similar magnitudes to previous lows during the latter 1990s (in contrast to the water vapor). One remarkable feature is that the 2001–02 anomalies are more persistent than prior cold periods in this (short) record.

Figure 14a shows the correlations between 82-hPa HALOE water vapor and cold point temperatures from each individual tropical radiosonde station (with a 2-month lag included to maximize correlations), and Fig. 14b shows a similar calculation based on 100-hPa temperatures from the ERA-40 data. Results from the gridded ERA-40 and station data are in good agreement, showing strongest correlations primarily for latitudes over ~10°N–10°S. This demonstrates that stratospheric water vapor anomalies are correlated primarily with temperatures near the equator. There is relatively little zonal structure to the positive equatorial correlations in Fig. 14, with slightly higher values in the eastern hemisphere, and near the date line.

Figure 15 compares the observed anomalies in HALOE 82-hPa $H_2O$ with anomalies in saturation mixing ratio ($Q_{sat}$) calculated from the tropical radiosonde cold point data (based on monthly means, which will probably overestimate minimum values, e.g., Dessler 1998). Overall there is reasonable correlation (as expected from the temperature comparisons), but the observed anomalies are substantially less than those in $Q_{sat}$ (the rms values are 0.27 and 0.90, respectively). One possible explanation for this difference is that, while the temperature anomalies occur primarily over 10°N–10°S (Fig. 14), the $H_2O$ anomalies are quickly transported

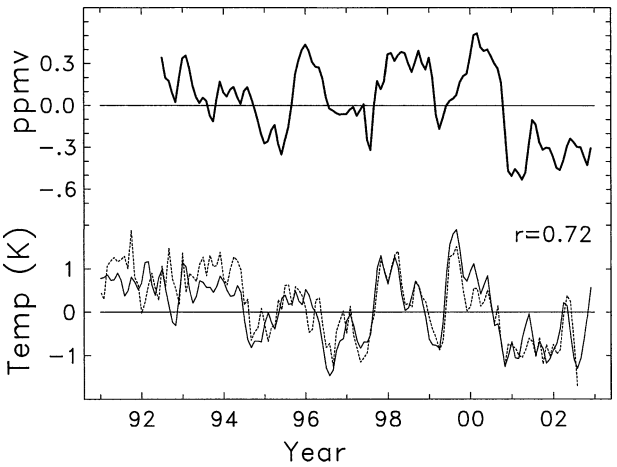


FIG. 13. (top) Time series of deseasonalized HALOE $H_2O$ at 82 hPa over 20°N–20°S (i.e., the near-bottom level in Fig. 2). (bottom) Deseasonalized anomalies in radiosonde cold point tropopause temperature, averaged from all stations over over 10°N–10°S (solid line), together with anomalies in ERA-40 100-hPa temperatures (dashed line). The $r = 0.72$ correlation refers to the water vapor and radiosonde temperature time series.

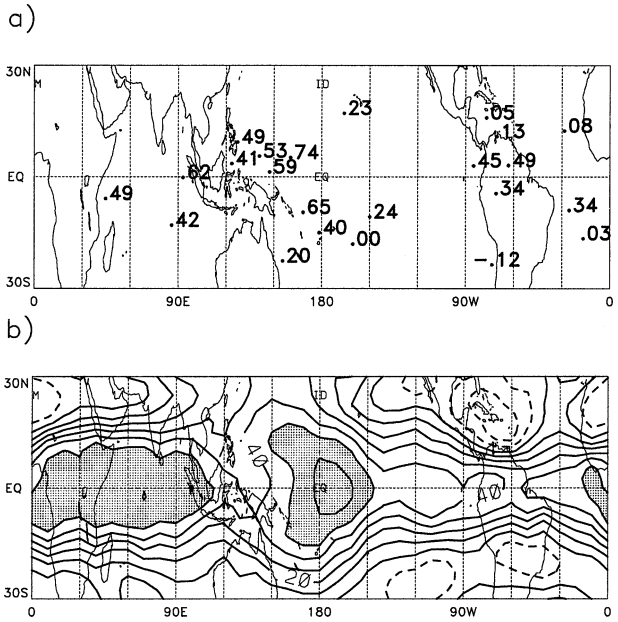


FIG. 14. (a) Numbers show the correlation between 82-hPa HALOE water vapor anomalies over 20°N–20°S (top of Fig. 13) with cold point tropopause temperature at each individual radiosonde station (with water vapor lagged by 2 months to maximize the correlations). (b) Map of correlation between 82-hPa water vapor and 100-hPa temperature anomalies from ERA-40 data. Contour interval is 0.1, with values above 0.5 shaded.

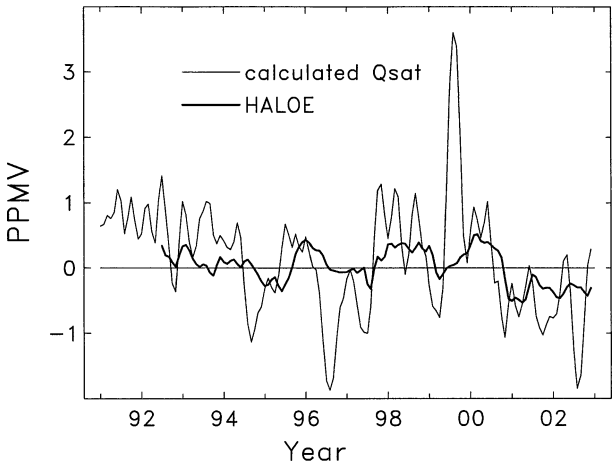


FIG. 15. Comparison of observed HALOE 82-hPa $H_2O$ anomalies over 20°N–20°S (dark line) with $H_2O$ saturation mixing ratio anomalies calculated from cold point tropopause temperature statistics (light line).

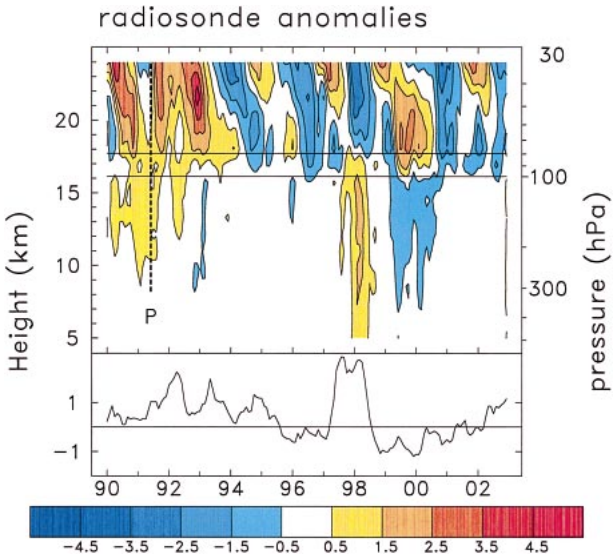


FIG. 16. Height–time section of interannual temperature anomalies in the Tropics for 1990–2002, derived from radiosonde data over 10°N–10°S. The cold point typically lies within the 100–80-hPa layer, noted by the horizontal lines. The time series at the bottom is the multivariate ENSO index, obtained from the Climate Diagnostics Center Web site (http://www.cdc.noaa.gov); P denotes the volcanic eruption of Mt. Pinatubo in Jun 1991.

over latitudes ~40°N–40°S (see Figs. 4–5), so that the effect of the tropical temperature anomalies is effectively diluted.

The vertical structure of the tropical temperature anomalies during 1990–2002 derived from radiosonde data (over 10°N–10°S) is shown in Fig. 16; this is intended to illustrate the processes that influence temperatures near the cold point (roughly the layer over 100–80 hPa). The largest tropical temperature anomalies occur in the stratosphere, with an approximate 2-yr periodicity and downward phase progression that are signatures of the stratospheric QBO. The bottom of the QBO temperature signal reaches near the cold point; for long-term statistics, the QBO magnitude at the tropopause is ~±0.5 K (Angell and Korshover 1964; Randel et al. 2000). Note that the QBO temperature signal is centered on the equator with an *e*-folding scale of approximately 10° latitude (Baldwin et al. 2001), so that the QBO mechanism is consistent with the equatorial maximum in temperature correlations shown in Fig. 14. A second source of stratospheric temperature variability in Fig. 16 is the Mt. Pinatubo volcanic eruption in June 1991, which resulted in warm temperature anomalies for approximately 2 yr, but with relatively small effects near the tropopause. Figure 16 also shows the effects of the large 1997–98 ENSO event, which warmed the tropical upper troposphere by ~2 K. This warming extended in altitude to above 100 hPa, contributing to the relatively warm tropopause region in 1997–98 (see Fig. 13). Thus both stratospheric and tropospheric meteorological processes contribute to temperature variability in the near-tropopause region, which in turn modulates stratospheric water vapor.

The near-global patterns of stratospheric water vapor fields influenced by tropical temperature anomalies are shown in Fig. 17. These show the correlations between radiosonde cold point temperature anomalies and HALOE $H_2O + 2 \times CH_4$ fields for time lags of 0, 6, and 12 months. The contemporaneous (lag 0) patterns show significant correlations in the lowest altitudes near the tropopause, with a meridional scale over ~30°N–30°S. At lag 6 months, the patterns of strongest correlations have risen in altitude by a few kilometers, and spread widely in latitude, covering nearly the entire globe over 60°N–60°S. Further vertical propagation is observed at lag 12 months, with strongest correlations observed in the NH.

## 6. Summary and discussion

Over 12 yr of continuous, near-global measurements of stratospheric water vapor are available from HALOE, and these data allow us to test our understanding of processes that control interannual changes, especially the influence of tropical tropopause temperatures. The HALOE $H_2O$ data show coherent interannual changes of magnitude ~±0.3 ppmv, with an approximate 2-yr periodicity. The anomalies originate near the tropical tropopause, and propagate vertically and latitudinally to influence much of the global stratosphere. The vertical propagation observed in Figs. 2–3 is the interannual analog of the seasonal tape recorder of Mote et al. (1996), with a mean upward velocity of ~8 km $yr^{-1}$. Likewise, the interannual anomalies in the lower stratosphere that originate in the Tropics propagate into middle and high latitudes of both hemispheres with a time scale of several months (Figs. 4–5). The HALOE data also show remarkably low and persistent $H_2O$ anomalies

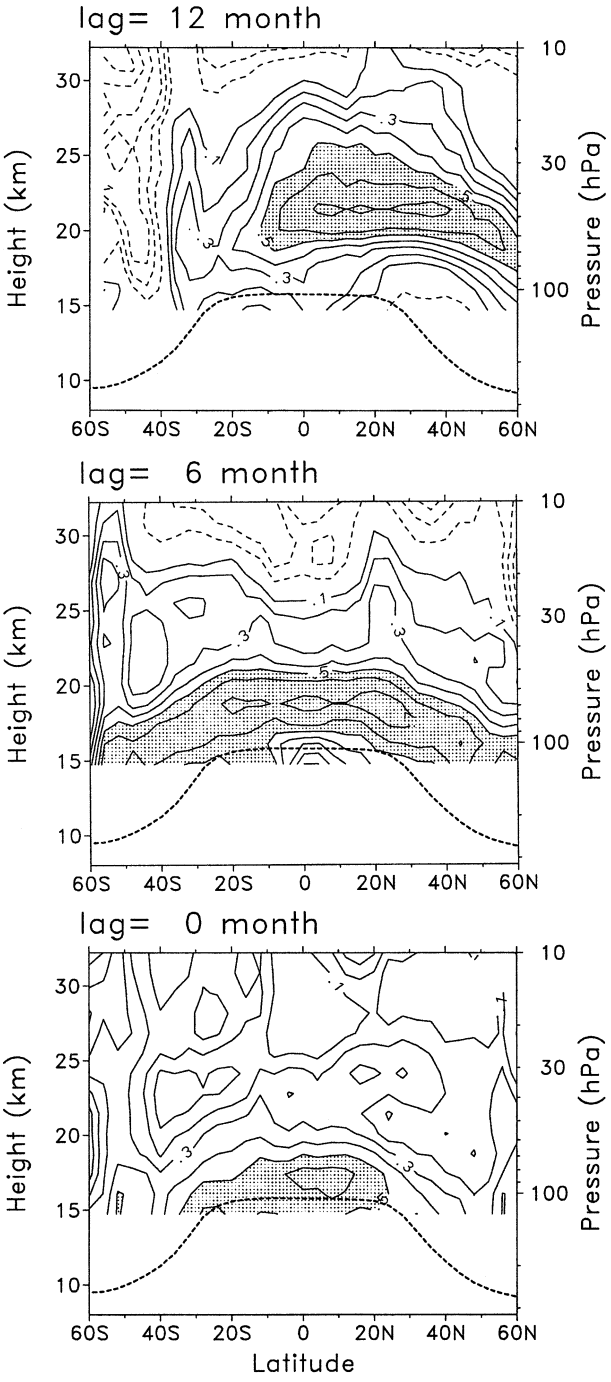


FIG. 17. Meridional cross sections of correlation between radiosonde tropical tropopause temperature anomalies (bottom of Fig. 13), and HALOE $H_2O + 2 \times CH_4$ anomalies at each latitude and height. Results are shown for time lags zero (bottom), 6 months (middle), and 12 months (top). Contours are $\pm 0.1, 0.2, \ldots$, with values above 0.5 shaded.

for the most recent 3 yr of the record (2001–03), and these low values cover much of the globe for this period.

The POAM satellite instrument has been making measurements of stratospheric water vapor over polar latitudes (~55°–70°N and ~65°–85°S) since 1998, allowing direct comparisons with HALOE for 1998–2003. Variations in lower-stratospheric water vapor over the Arctic are dominated by transport from tropical latitudes for both seasonal (Randel et al. 2001; Nedoluha et al. 2002) and interannual variations (see Fig. 4), while in situ dehydration dominates over Antarctica (e.g., Nedoluha et al. 2000). Direct comparison of the POAM and HALOE data over the Arctic shows remarkably good agreement for interannual anomalies (Fig. 7), including persistent low values after 2001. The interannual consistency between these two independent datasets promotes confidence in the global HALOE record.

The most continuous long-term record of stratospheric water vapor is from balloon-borne frost-point hygrometer measurements made at Boulder, Colorado (40°N), since 1980, and these data invite detailed comparisons with the HALOE record since 1992. Comparisons with HALOE data near Boulder (Fig. 8) show reasonable agreement for the early part of the overlap record (1992–96). However, the time series in Fig. 8 diverge after 1997, with balloon data increasing in time, but HALOE staying relatively constant or decreasing (note, however, that certain aspects of interannual variability in Fig. 8 are consistent, most notably the relatively low values for 2001–02 seen in both datasets). The reason for this difference in the datasets after 1997 is unclear at present, but the result is that calculated decadal-scale changes (trends) for 1992–2002 are very different between the balloon and satellite datasets: the Boulder balloon data show increases of ~0.5%–1% $yr^{-1}$ whereas HALOE shows small or negative trends in the lower stratosphere (Fig. 9). The HALOE trends are not representative of long-term monotonic changes, but are clearly influenced by end points of the short data record (see Fig. 10). The reason(s) for the disparity between the Boulder balloon and HALOE satellite water vapor data after 1997, and the differences in the respective long-term changes, are unknown at present. It will be important to reconcile these data, as they are the two longest and most continuous records available for stratospheric water vapor.

A key focus of this work is quantifying the relationship between the observed HALOE $H_2O$ changes in the lower stratosphere and temperatures near the tropical tropopause (which can simply modulate the seasonal freeze drying of air entering the tropical stratosphere). We have noted substantial uncertainty in estimates of interannual temperature variability near the tropical tropopause, and have considered results based on six different data sources (NCEP–NCAR and ERA-40 reanalyses, CPC and METO stratospheric analyses, and radiosondes and GPS data, the latter only for 1995–97 and 2001–02). While there is reasonable agreement between the different datasets in the tropical lower stratosphere (50 and 70 hPa), there are important differences at 100 hPa. In particular, the NCEP–NCAR and METO data show large and persistent cold anomalies of 2–3 K

at 100 hPa during 2001–02, which are not seen in ERA-40, CPC, radiosonde, or GPS data (Fig. 11). These 100-hPa differences for 2001–02 are especially troublesome because this is the time period of the observed low $H_2O$ anomalies in the HALOE record (and these would match well with the cold NCEP–NCAR and METO 100-hPa anomalies). However, comparison of the different datasets with MSU-4 satellite measurements (Fig. 12) and examination of the anomaly vertical profiles (not shown here) cast suspicion on the METO and NCEP–NCAR results. Furthermore, there are known changes in analysis systems and input data that likely influence continuity in these data, and we do not include the NCEP–NCAR and METO data in further analyses.

Anomalies in tropical tropopause temperatures derived from radiosondes and ERA-40 reanalyses are strongly correlated with HALOE $H_2O$ (Fig. 13). Radiosonde data show that the strongest correlations occur using the cold point tropopause. The spatial pattern of correlations (Fig. 14) suggest that temperatures in the deep Tropics (~10°N–10°S) most strongly influence lower-stratospheric water vapor, and there is not strong zonal structure to the correlations. The meridional scale of ~10°N–10°S, lack of zonal structure, and approximate 2-yr periodicity are consistent with a predominant QBO influence. While the $H_2O$ saturation mixing ratio anomalies calculated from temperatures over 10°N–10°S are substantially larger than observed (Fig. 15), this can be reconciled by the observed latitudinal spreading of the tropical signal to ~40°N–40°S, so that the forced tropical signal is ''diluted.'' The observation that interannual changes in water vapor are closely linked to large-scale temperature variations near the tropopause is consistent with the idealized modeling studies of tropical dehydration of Holton and Gettelman (2001), Gettelman et al. (2002), and Jensen and Pfister (2004).

The persistent low $H_2O$ anomalies seen during 2001–03 in HALOE data are less easy to understand. As a whole, tropical tropopause temperatures are cold for this period, but not unusually cold compared to prior minima during the 1990s (Fig. 13). One remarkable aspect of the temperatures during this time is that they remain relatively cold for an extended period (approximately 2 yr), whereas prior cold periods had shorter duration. Because stratospheric water vapor responds in an integrated manner to tropopause temperatures, the extended cold tropopause during 2001–02 may be one source of the unusually low water vapor during these years. Other factors, such as the detailed vertical structure of temperatures near the cold point, changes in tropical deep convection or changes in dehydration microphysics, may also be important.

The downward vertical propagation of stratospheric temperature anomalies, their ~2-yr periodicity, and near-equatorial latitudinal structure all implicate the QBO as a mechanism influencing near-tropopause temperatures (and hence $H_2O$). This QBO influence on stratospheric $H_2O$ has been analyzed in numerical simulations by Giorgetta and Bengston (1999) and Geller et al. (2002). The detailed time variations of tropical temperatures (Fig. 16) furthermore suggest that the strong tropospheric ENSO ''warm event'' during 1997–98 also had an influence on the tropopause, and was partially responsible for the positive stratospheric $H_2O$ anomalies observed during this time. The primary effect of a ''warm'' ENSO event on the tropical tropopause is a dipole pattern of temperature anomalies in the western and central Pacific, so that the climatological minimum temperatures are somewhat warmer (Gettelman et al. 2001). The resulting influence on stratospheric water vapor has been simulated by Geller et al. (2002) and Scaife et al. (2003), with results similar to the observations here.

*Acknowledgments.* We thank Wesley Ebisuzaki, Bob Kistler, Kevin Trenberth, and Richard Swinbank for discussions regarding the NCEP–NCAR reanalysis and METO datasets; Martin McHugh, Ellis Remsberg, and Earl Thompson for input on HALOE data quality; and Andy Dessler, Rolando Garcia, Philip Mote, and Darryn Waugh for discussions and comments on the manuscript. Constructive reviews and suggestions for improvement were provided by James Russell III, Dian Seidel, and Xuelong Zhou. This work has been partially supported by the NASA Atmospheric Chemistry Modeling and Analysis Program (ACMAP). Marilena Stone expertly prepared the manuscript. NCAR is sponsored by the National Science Foundation.

## REFERENCES

Angell, J. K., and J. Korshover, 1964: Quasi-biennial variations in temperature, total ozone, and tropopause height. *J. Atmos. Sci.,* **21,** 479–492.

Baldwin, M. A., and Coauthors, 2001: The quasi-biennial oscillation. *Rev. Geophys.,* **39,** 179–229.

Brewer, A. W., 1949: Evidence for a world circulation provided by measurements of helium and water vapor distribution in the stratosphere. *Quart. J. Roy. Meteor. Soc.,* **75,** 351–363.

Christy, J. R., R. W. Spencer, and W. D. Braswell, 2000: MSU tropospheric temperatures: Dataset construction and radiosonde comparisons. *J. Atmos. Oceanic Technol.,* **17,** 1153–1170.

Danilin, M. Y., and Coauthors, 2002: Comparison of ER-2 aircraft and POAM III, MLS, and SAGE II satellite measurements during SOLVE using traditional correlative analysis and trajectory hunting technique. *J. Geophys. Res.,* **107,** 8315, doi:10.1029/2001JD000781.

Dessler, A. E., 1998: A reexamination of the 'stratospheric fountain' hypothesis. *Geophys. Res. Lett.,* **25,** 4165–4168.

——, E. Weinstock, E. Hintsa, J. Anderson, C. Webster, R. May, J. Elkins, and G. Dutton, 1994: An examination of the total hydrogen budget of the lower stratosphere. *Geophys. Res. Lett.,* **21,** 2563–2566.

Dvortsov, V. L., and S. Solomon, 2001: Response of the stratospheric temperatures and ozone to past and future increases in stratospheric humidity. *J. Geophys. Res.,* **106,** 7505–7514.

Elliot, W. P., R. J. Ross, and W. H. Blackmore, 2002: Recent changes in NWS upper-air observations with emphasis on changes from VIZ to Vaisala radiosondes. *Bull. Amer. Meteor. Soc.,* **83,** 1003–1017.

Forster, P. M. D., and K. P. Shine, 1999: Stratospheric water vapour

changes as a possible contributor to observed stratospheric cooling. *Geophys. Res. Lett.,* **26,** 3309–3312.
Geller, M. A., X. Zhou, and M. Zhang, 2002: Simulations of the interannual variability of stratospheric water vapor. *J. Atmos. Sci.,* **59,** 1076–1085.
Gelman, M. E., A. J. Miller, K. W. Jihnson, and R. N. Nagatani, 1986: Detection of long term trends in global stratospheric temperature from NMC analyses derived from NOAA satellite data. *Adv. Space Res.,* **6,** 17–26.
Gettelman, A., W. J. Randel, S. Massie, F. Wu, W. G. Read, and J. M. Russell, 2001: El Niño as a natural experiment for studying the tropical tropopause region. *J. Climate,* **14,** 3375–3392.
——, ——, F. Wu, and S. T. Massie, 2002: Transport of water vapor in the tropical tropopause layer. *Geophys. Res. Lett.,* **29,** 1009, doi:10.1029/2001GL012818.
Giorgetta, M. A., and L. Bengston, 1999: Potential role of the quasi-biennial oscillation in the stratosphere–troposphere exchange as found in water vapor in general circulation model experiments. *J. Geophys. Res.,* **104,** 6003–6019.
Hajj, G. A., and Coauthors, 2004: CHAMP and SAC-C atmospheric occultation results and intercomparisons. *J. Geophys. Res.,* **109,** D06109, doi:10.1029/2003JD003909.
Harries, J. E., and Coauthors, 1996: Validation of measurements of water vapor from the Halogen Occultation Experiment, HALOE. *J. Geophys. Res.,* **101,** 10 205–10 216.
Hervig, M., J. M. Russell, L. L. Gordlen, T. Daniels, S. R. Drayson, and J. H. Park, 1995: Aerosol effects and corrections in the HALOGEN Occultation Experiment. *J. Geophys. Res.,* **100,** 1067–1079.
Holton, J. R., and A. Gettelman, 2001: Horizontal transport and the dehydration of the stratosphere. *Geophys. Res. Lett.,* **28,** 2799–2802.
Jensen, E., and L. Pfister, 2004: Transport and freeze-drying in the tropical tropopause layer. *J. Geophys. Res.,* **109,** D02207, doi:10.1029/2003JD004022.
Kalnay, E., and Coauthors, 1996: The NCAR/NCEP 40-Year Reanalysis Project. *Bull. Amer. Meteor. Soc.,* **77,** 437–471.
Kistler, R., and Coauthors, 2001: The NCEP–NCAR 50-year reanalysis: Monthly means CD-ROM and documentation. *Bull. Amer. Meteor. Soc.,* **82,** 247–267.
Kley, D. J., M. Russell III, and C. Phillips, Eds., 2000: SPARC Assessment of Upper Tropospheric and Stratospheric Water Vapor. SPARC Tech. Rep. 2, 312 pp.
Kursinski, E. R., and Coauthors, 1996: Initial results of radio occultation observations of Earth's atmosphere using the global positioning system. *Science,* **271,** 1107–1110.
Lanzante, J. R., S. A. Klein, and D. J. Seidel, 2003: Temporal homogenization of monthly radiosonde temperature data. Part I: Methodology. *J. Climate,* **16,** 224–240.
Lorenc, A., and Coauthors, 2000: The Met Office global 3-dimensional variational data assimilation scheme. *Quart. J. Roy. Meteor. Soc.,* **126,** 2992–3012.
Lucke, R. L., and Coauthors, 1999: The Polar Ozone and Aerosol Measurement (POAM) III instrument and early validation results. *J. Geophys. Res.,* **104,** 18 785–18 799.
Lumpe, J. D., R. M. Bevilacqua, K. W. Hoppel, and C. E. Randell, 2002: POAM III retrieval algorithm and error analysis. *J. Geophys. Res.,* **107,** 4575, doi:10.1029/2002JD002137.
Mears, C. A., M. C. Schabel, and F. J. Wentz, 2003: A reanalysis of the MSU channel 2 tropospheric temperature record. *J. Climate,* **16,** 3650–3664.
Mote, P. W., K. H. Rosenlof, J. R. Holton, R. S. Harwood, and J. W. Waters, 1996: An atmospheric tape recorder: The imprint of tropical tropopause temperatures on stratospheric water vapor. *J. Geophys. Res.,* **101,** 3989–4006.
——, T. J. Dunkerton, M. E. McIntyre, E. A. Ray, P. H. Haynes, and J. M. Russell III, 1998: Vertical velocity, vertical diffusion, and dilution by midlatitude air in the tropical lower stratosphere. *J. Geophys. Res.,* **103,** 8651–8666.
Nedoluha, G. E., R. M. Bevilacqua, R. M. Gomoz, D. E. Siskind, and B. C. Hicks, 1998: Increases in middle atmospheric water vapor as observed by the Halogen Occultation Experiment and the ground-based Water Vapor Millimeter-Wave Spectrometer from 1991 to 1997. *J. Geophys. Res.,* **103,** 3531–3543.
——, and Coauthors, 2000: POAM III measurements of dehydration in the Antarctic lower stratosphere. *Geophys. Res. Lett.,* **27,** 1683–1686.
——, R. M. Bevilacqua, K. W. Hoppel, J. D. Lumpe, and H. Smit, 2002: Polar Ozone and Aerosol Measurement III measurements of water vapor in the upper troposphere and lowermost stratosphere. *J. Geophys. Res.,* **107,** 4103, doi:10.1029/2001JD000793.
——, ——, R. M. Gomez, B. C. Hicks, J. M. Russell III, and B. J. Connor, 2003: An evaluation of trends in middle atmospheric water vapor as measured by HALOE, WVMS, and POAM. *J. Geophys. Res.,* **108,** 4391, doi:10.1029/2002JD003332.
Niwano, M., K. Yamazaki, and M. Shiotani, 2003: Seasonal and QBO variations in ascent rate in the tropical lower stratosphere as inferred from UARS HALOE trace gas data. *J. Geophys. Res.,* **108,** 4794, doi:10.1029/2003JD003871.
Oltmans, S. J., H. Volmel, D. J. Hofmann, K. Rosenlof, and D. Kley, 2000: The increase in stratospheric water vapor from balloon borne frostpoint hygrometer measurements at Washington, D. C. and Boulder, Colorado. *Geophys. Res. Lett.,* **27,** 3453–3456.
Park, J. H., and Coauthors, 1996: Validation of HALOE $CH_4$ measurements from UARS. *J. Geophys. Res.,* **101,** 10 183–10 204.
Pawson, S., and M. Fiorino, 1999: The tropical lower stratosphere in atmospheric reanalyses. Part 3: Inclusion of the pre-satellite data era. *Climate Dyn.,* **15,** 241–250.
Randel, W. J., F. Wu, and J. M. Russell III, 1998: Seasonal cycles and QBO variations in stratospheric $CH_4$ and $H_2O$ observed in UARS HALOE data. *J. Atmos. Sci.,* **55,** 163–185.
——, ——, ——, and J. Waters, 1999: Space–time patterns of trends in stratospheric constituents derived from UARS measurements. *J. Geophys. Res.,* **104,** 3711–3727.
——, ——, and D. J. Gaffen, 2000: Interannual variability of the tropical tropopause derived from radiosonde data and NCEP reanalyses. *J. Geophys. Res.,* **105,** 15 509–15 523.
——, ——, A. Gettelman, J. M. Russell III, J. M. Zawodny, and S. J. Oltmans, 2001: Seasonal variation of water vapor in the lower stratosphere observed in Halogen Occultation Experiment data. *J. Geophys. Res.,* **106,** 14 313–14 325.
Randel, W., M.-L. Chanin, and C. Michant, Eds., 2002: SPARC Intercomparison of Middle Atmosphere Climatologies. SPARC Tech. Rep. 3, 96 pp.
——, F. Wu, and W. R. Rios, 2003: Thermal variability of the tropical tropopause region derived from GPS/MET observations. *J. Geophys. Res.,* **108,** 4024, doi:10.1029/2002JD002595.
Remsberg, E. E., J. M. Russell III, L. L. Gordley, J. C. Gille, and P. L. Bailey, 1984: Implications of stratospheric water vapor distributions as determined from the NIMBUS 7 LIMS experiment. *J. Atmos. Sci.,* **41,** 2934–2945.
Rocken, C., and Coauthors, 1997: Analysis and validation of GPS/MET data in the neutral atmosphere. *J. Geophys. Res.,* **102,** 29 849–29 866.
Rosenlof, K. H., 1995: Seasonal cycle of the residual mean meridional circulation in the stratosphere. *J. Geophys. Res.,* **100,** 5173–5192.
——, 2002: Transport changes inferred from HALOE water and methane measurements. *J. Meteor. Soc. Japan,* **80,** 831–848.
Russell, J. M., III, A. F. Tuck, L. L. Gordley, J. H. Park, S. R. Drayson, J. E. Harries, R. J. Cicerone, and P. J. Crutzen, 1993: The HALOGEN Occultation Experiment. *J. Geophys. Res.,* **98,** 10 777–10 797.
Santer, B. D., J. Hnilo, T. M. Wigley, J. S. Boyle, C. Doutriaux, M. Fiorino, D. E. Parker, and K. E. Taylor, 1999: Uncertainties in observationally based estimates of temperature change in the free atmosphere. *J. Geophys. Res.,* **104,** 6305–6334.

Scaife, A. A., N. Buchart, D. R. Jackson, and R. Swinbank, 2003: Can changes in ENSO activity help explain increasing stratospheric water vapor? *Geophys. Res. Lett.*, **30,** 1880, doi:10.1029/2003GL017591.

Seidel, D. J., R. J. Ross, J. K. Angell, and G. C. Reid, 2001: Climatological characteristics of the tropical tropopause as revealed by radiosondes. *J. Geophys. Res.*, **106,** 7857–7878.

Sherwood, S. C., and A. E. Dessler, 2001: A model for transport across the tropical tropopause. *J. Atmos. Sci.,* **58,** 765–779.

Shine, K. P., and Coauthors, 2003: A comparison of model-simulated trends in stratospheric temperatures. *Quart. J. Roy. Meteor. Soc.*, **129,** 1565–1588.

Smith, W. L., H. M. Woolf, C. M. Haydex, D. Q. Wark, and L. W. McMill, 1979: The TIROS-N operational vertical sounder. *Bull. Amer. Meteor. Soc.,* **60,** 1177–1187.

Spencer, R. W., and J. R. Christy, 1993: Precision lower stratospheric temperature monitoring with the MSU: Technique, validation, and results 1979–1991. *J. Climate,* **6,** 1194–1204.

Swinbank, R., and A. O'Neill, 1994: A stratosphere–troposphere data assimilation system. *Mon. Wea. Rev.*, **122,** 686–702.

Trenberth, K. E., 1984: Some effects of finite sample size and persistence on meteorological statistics. Part I: Autocorrelations. *Mon. Wea. Rev.,* **112,** 2359–2368.

——, and J. G. Olson, 1988: Evaluation of NMC global analyses. NCAR Tech. Note NCAR/TN-299+STR, 82 pp.

Voemel, H., S. J. Oltmans, D. J. Hofmann, T. Deshler, and J. M. Rosen, 1995: The evolution of the dehydration in the Antarctic stratospheric vortex. *J. Geophys. Res.*, **100,** 13 919–13 926.

Waugh, D. W., and T. M. Hall, 2002: Age of stratospheric air: Theory, observations and models. *Rev. Geophys.,* **40,** 1010, doi:10.1029/2000RG000101.

Wickert, J., and Coauthors, 2001: Atmosphere sounding by GPS radio occultation: First results from CHAMP. *Geophys. Res. Lett.,* **28,** 3263–3266.

Zhou, X. L., M. A. Geller, and M. Zhang, 2001: Cooling trend of the tropical cold point tropopause temperatures and its implications. *J. Geophys. Res.,* **106,** 1511–1522.